

Lyman Break Galaxies Under a Microscope: The Small Scale Dynamics and Mass of an Arc in the Cluster 1E0657-56¹

N.P.H. Nesvadba², M.D. Lehnert², F. Eisenhauer², R. Genzel², S. Seitz², R.I. Davies², R.P. Saglia², D. Lutz², L. Tacconi², R. Bender², R. Abuter²

ABSTRACT

Using the near-infrared integral-field spectrograph SPIFFI on the VLT, we have studied the spatially-resolved dynamics in the $z = 3.2$ strongly lensed galaxy 1E0657-56 “arc+core” by observing the rest-frame optical emission lines [OIII] λ 5007 and H β . The lensing configuration suggests that the high surface brightness “core” is the $\mathcal{M} \sim 20$ magnified central ~ 1 kpc of the galaxy, whereas the fainter “arc” is the more strongly magnified peripheral region of the same galaxy at about a half-light radius, which otherwise appears to be a typical $z \sim 3$ Lyman break galaxy.

The overall shape of the position-velocity diagram resembles the “rotation curves” of the inner few kpcs of nearby $\sim \mathcal{L}^*$ spiral galaxies. For $\mathcal{M} = 20$, our data have a spatial resolution of ~ 200 pc in the source plane. The projected velocities $v_{rot,proj}$ rise rapidly to ~ 75 km s⁻¹ within radii ~ 0.5 kpc from the center, and asymptotically reach a velocity of ~ 190 km s⁻¹ within the arc, at a projected radius of a few kpc radius. The rotation curve implies a dynamical mass of $\log M_{dyn}/M_{\odot} \sim 9.3$ within the central kpc, and suggests that in this system the equivalent of the mass of a present-day $\sim \mathcal{L}^*$ bulge at the same radius was already in place by $z \gtrsim 3$. Approximating the circular velocity of the halo by the measured asymptotic velocity of the rotation curve, we estimate a dark matter halo mass of $\log M_{halo}/M_{\odot} \sim 11.7 \pm 0.3$, in good agreement with large-scale clustering studies of Lyman break galaxies. The baryonic collapse fraction is low compared to $z \sim 2$ actively star-forming “BX” and low-redshift galaxies, perhaps implying comparatively less gas infall to small radii or efficient feedback. Even more speculatively, the high central mass density might indicate highly dissipative gas collapse in very early stages of galaxy evolution, in approximate agreement with what is expected for “inside-out” galaxy formation models.

¹Based on observations collected at the European Southern Observatory, Very Large Telescope Array, Cerro Paranal; program numbers, 70.B-0545(A) and 70.A-0229(A)

²Max-Planck-Institut für extraterrestrische Physik, Giessenbachstraße, 85748 Garching bei München, Germany

Subject headings: cosmology: observations — galaxies: evolution — galaxies: kinematics and dynamics — infrared: galaxies

1. Introduction

Dynamical mass estimates of high redshift galaxies are now starting to play a significant role in our developing understanding of galaxy assembly in the early universe, a trend that will likely become even more important in the near future. Directly measuring the dynamical masses from the spatially-resolved spectra of high-redshift galaxies is observationally very challenging, but dynamical masses are less prone to degeneracies and evolutionary bias than mass estimates based solely on photometry. Fascinatingly, they may also allow us to directly probe the baryonic and dark matter content and concentration of galaxies in the early universe, and to measure their angular momenta (Förster Schreiber et al. 2006). Ultimately, they will enable us, for example, to directly compare the growth of galaxy mass and angular momentum with model predictions as a function of redshift. Accurately measuring the kinematics of high-redshift galaxies is therefore a major step forward.

To realize these goals, we must show convincingly that the kinematics we measure in a high redshift galaxy have a simple proportionality to the mass distribution and rule out that they are dominated by the orbit or angular momentum loss of mergers or by hydrodynamical processes like, e.g., starburst-driven “superwinds” (Lehnert & Heckman 1996a).

The Lyman-break technique has led to the largest sample of spectroscopically confirmed galaxies from $z \sim 2.7$ to 6.4. Despite our rapidly growing understanding of their ensemble properties, such as their luminosity function, clustering, and star-formation history (e.g., Steidel et al. 1996; Adelberger et al. 1998), our knowledge of their detailed intrinsic properties remains rather rudimentary. LBGs at $z \sim 3$ have typical radii of $r_e \sim 0.3''$ (Giavalisco, Steidel, & Macchetto 1996) so that the spatially resolved kinematics are often difficult to obtain. Thus, dynamical mass estimates for individual LBGs at $z \sim 3$ (e.g., Pettini et al. 2001) are based mostly on line widths and only in a handful of cases have velocity gradients been observed. Spatially resolved LBGs are large compared to the overall population, and might be biased towards the strongest line emitting galaxies (e.g., vigorous starbursts) or early-stage mergers and perhaps are not representative for the overall population.

The only way to properly address these issues is to resolve the dynamics of an LBG on fine scale. Strongly gravitationally lensed LBGs are a promising way to probe small physical scales even with seeing-limited data. The ideal target would be a strongly-lensed, highly inclined LBG, where the kinematic major axis is roughly along a caustic. Such a

configuration would allow several patches of the same galaxy, but at different radii, to be highly magnified to include the intrinsically low surface-brightness periphery. Probing non-lensed LBGs in this way is impossible given their generally small radii, faint magnitudes, and low surface brightnesses.

Unfortunately, strongly lensed LBGs with a favorable lensing geometry are exceedingly rare. Two cases at $z > 1$ have been studied in detail so far, MS1512-cB58 at $z=2.8$ (e.g., Teplitz et al. 2000; Pettini et al. 2002; Baker et al. 2004) and AC114-S2 at $z=1.9$ (Lemoine-Busserolle et al. 2003). However, the underlying dynamical mechanism is not conclusively revealed in either case. MS1512-cB58 is magnified by a factor ~ 30 , but it is compact and has no apparent velocity gradient (Teplitz et al. 2000) – most likely because of an unfavourable lensing geometry. From the mm CO emission line width, Baker et al. (2004) measure $M_{dyn} \sim 10^{10} M_{\odot}$, not corrected for inclination. AC114-S2 has a velocity gradient (Lemoine-Busserolle et al. 2003), but is a merger with complex morphology, and its nature is not well constrained. That spatially-resolved spectroscopy of giant arcs can provide valuable constraints on the internal dynamics of the lensed galaxies has recently been shown by Swinbank et al. (2006) for a sample of 6 giant arcs at lower redshift, $z \sim 1$. Swinbank et al. found regular kinematics in 4 of the 6 galaxies, consistent with quiescently rotating disks, while in 2 galaxies, they observed complex line profiles of varying widths and irregular velocity structure suggestive of either mergers or outflows.

The strongly lensed $z=3.24$ ¹ “arc+core” galaxy behind the $z=0.3$ X-ray cluster 1E0657-56 (Tucker et al. 1998) appears to be different from these well-studied high-redshift gravitational arcs. Its lensing configuration suggests the simultaneous magnification of a high surface brightness region at the south-eastern tip of the source that may be associated with the “core” of the galaxy as well as a more highly magnified, lower surface brightness region outside the core (“arc”; Mehlert et al. 2001). The total extent of the arc is $\sim 14''$, and it has a complex substructure: Mehlert et al. (2001) identify 3 faint knots of similar surface brightness within the arc, each separated by a few arcseconds. They propose that the central highest surface brightness region of the lensed galaxy, lying near, but outside the cusp-caustic, is seen as the bright core, whereas a fainter outer region on one side of the same galaxy, which touches the cusp-caustic and is split into three merging images, constitutes the full extent of the arc. Thus the asymmetric magnified image comprising the near-nuclear region and peripheral patches originating on one side of the galaxy. The high magnification ($\mathcal{M} \gtrsim 20$) presents an excellent opportunity to investigate the properties of a $z \sim 3$ galaxy at

¹We adopt a flat concordance cosmology with $\Omega_{\Lambda}=0.7$ and $H_0=70 \text{ km s}^{-1} \text{ Mpc}^{-1}$, in which $D_L=27.9 \text{ Gpc}$ and $D_A=1.5 \text{ Gpc}$ at $z = 3.24$. The size scale is $7.5 \text{ kpc}''$. The age of the universe at this redshift and cosmological model is 1.9 Gyrs.

different radii with high physical and spatial resolution.

The paper is organized as follows: After presenting observations and data reduction in §2, we turn in §3 to the rest-frame UV and optical properties, highlighting the high-resolution ACS morphology. We discuss the spatially-resolved rest-frame emission line kinematics extracted from three-dimensional data cubes obtained with the integral-field spectrograph SPIFFI in §4. This includes a detailed discussion of the 146 km s^{-1} velocity gradient in the core and its continuation in the arc. In §5, we present a detailed comparison with the internal dynamics of low-redshift spiral galaxies. In §6, we estimate the evolution and angular momentum of the arc+core, before investigating the halo mass and the baryonic “collapse fraction” in §7. We summarize our results in §8 and draw a likely evolutionary scenario for LBGs.

2. Observations and Data Reduction

Given the interesting lensing configuration of the 1E0657-56 arc+core galaxy and the wealth of supplementary data, we observed it with the near-infrared integral field spectrograph SPIFFI (Eisenhauer et al. 2000), using UT2 of the VLT (SPIFFI has since become part of the SINFONI instrument on UT4). We obtained deep K band spectroscopy of 1E0657-56 arc core, covering the core and neighboring parts of the arc. Observations in April 2003 were carried out under variable sky conditions, with a total integration time of 190 minutes. One “off” frame at a sky position was taken for each “on” frame in an off-on-on-off mode, with a spectral resolution of $R \sim 2400$ at $2.2 \mu\text{m}$ and using the scale of $0.25'' \text{ pixel}^{-1}$. Individual exposure times are 600s.

Data reduction was performed extending the package of the standard IRAF (Tody 1993) tools for reducing longslit spectra. Individual exposures were dark frame subtracted and flat-fielded using exposures of an internal calibration lamp. We identified bad pixels based on dark and flat-field frames, and replaced them by interpolations of the surrounding pixels (in all 3 dimensions). Rectification and wavelength calibration are done before night sky subtraction, to account for some spectral flexure between the frames. Curvature in each individual slit-let of each frame was measured and removed using an arc lamp, before shifting the spectra to an absolute (vacuum) wavelength scale with reference to the OH lines in the data.

To account for variations in the night sky emission, we normalize the sky frame to the average of the object frame separately for each wavelength before sky subtraction, masking bright foreground objects, and correcting for residuals of the background subtraction and

uncertainties in the flux calibration by subsequently subtracting the (empty sky) background separately from each wavelength plane.

The three dimensional data cubes are then reconstructed, assuming that each slitlet covers exactly 32 pixels. They are spatially aligned by cross-correlating the collapsed cubes, and then combined, clipping deviant pixels. Telluric correction is applied to the combined cube. Flux scales are obtained from standard star observations. From the light profile of the standard star, we measure the FWHM spatial resolution to be $0.6'' \times 0.4''$ in right ascension and declination, respectively.

Data taking and reduction of the rest-frame UV spectroscopy of the arc and core with FORS1 on the VLT was described by Mehlert et al. (2001). They also kindly provided their R-band data for the present work, which has a total exposure time of 3800 s and seeing of $0.6'' - 0.9''$. Mehlert et al. (2001) give a full account of how these data were obtained and reduced. C. Forman-Jones and collaborators have recently obtained high-resolution imaging of the cluster 1E0657-56 through the F814W filter using the ACS camera onboard the HST. They kindly shared with us a portion of their full image containing the region around the arc+core before publication.

3. High-resolution rest-frame UV Morphology

The ACS F814W image ($\sim 2000\text{\AA}$ in the rest-frame) shows the complex structure of this source in great detail (Fig. 1). Irregular high surface-brightness patches, perhaps star-forming HII regions, are seen in the arc, embedded in a more continuous structure with much lower surface brightness. The core has an overall higher surface brightness, with a bright, unresolved spot in the center, and two extensions of lower surface brightness in an S-like shape.

The spatial resolution of the image (obtained from the TinyTim package; Krist & Hook 1997) is $0.09''$ in both right ascension and declination. The arc and core are both spatially resolved in the direction perpendicular to the magnification axis. Deconvolved profile widths along the unlensed direction are $0.113''$ (~ 0.9 kpc) for the brightest part of the core, and $\sim 0.3 - 0.6''$ ($2.4 - 4.8$ kpc) in the arc. Along the magnification axis, the central region of the core has a diameter of $\sim 0.4''$, about 4 times larger than the unlensed $0.113''$ diameter perpendicular to it.² The full size of the core along the direction of magnification is $1.3''$.

²Strictly speaking, this is true only if the gravitational lens has an isothermal dark matter halo mass profile. However, the arc+core galaxy lies near the Einstein radius, so the exact profile shape does not have

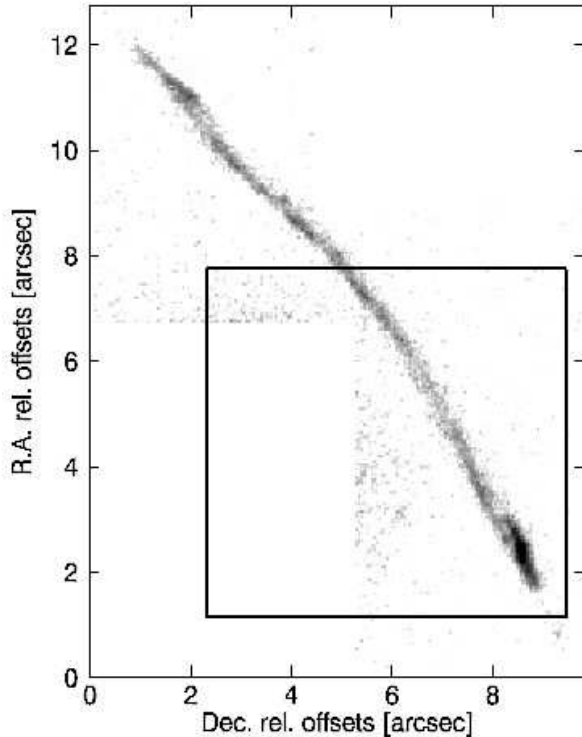


Fig. 1.— ACS F814W image of the whole arc+core. The core is the relatively high surface brightness region at the bottom right-hand corner in the image, while the arc is the lower surface brightness region that extends to the north-east of the core. North is at the top, and east is to the left in this image. The box indicates the SPIFFI field of view of our data cube. The ACS data were kindly provided by C. Forman-Jones.

4. Spatially-Resolved Spectroscopy and Internal Kinematics

Since the lensing direction is roughly along the vertical axis of the cube, and the SPIFFI data are not spatially resolved in the perpendicular direction, we simply extract spectra from each individual pixel row or slitlet which lie along this direction. The core is a bright [OIII] λ 5007 line emitter, with $S/N = 10 - 20$ in each spectrum, and uniform dispersions of $\sigma \sim 70 \text{ km s}^{-1}$. Fitting the centroids of the [OIII] λ 5007 emission line, we find an overall velocity gradient of 146 km s^{-1} over a total physical distance of $0.9h_{70}^{-1} \text{ kpc}$ for $\mathcal{M} = 20$. Extracting spectra from the 3 knots indicated by the boxes in Fig. 2 yields offsets relative to the core of $\Delta v_{knot1} = -104 \pm 8 \text{ km s}^{-1}$, $\Delta v_{knot2} = -152 \pm 9 \text{ km s}^{-1}$, and $\Delta v_{knot3} = -239 \pm 7$

much of an impact on this estimate.

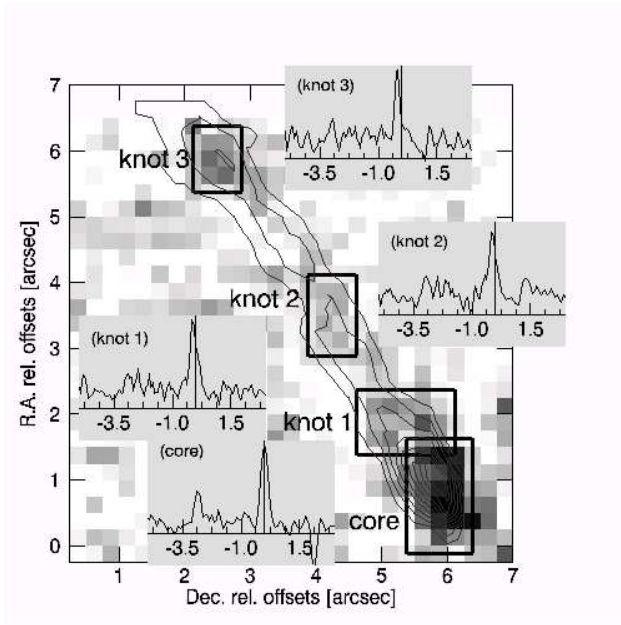


Fig. 2.— Continuum subtracted, combined $[\text{OIII}]\lambda\lambda 4959,5007$ line image of 1E0657 arc and core (*shown as greyscale*). Contours show the distribution of the rest-frame UV surface brightness from the R-band image (kindly provided by Mehlert et al. 2001). Spectra, extracted from the rectangular regions as indicated on the image, of areas in the arc and core are shown in the insets. The velocities indicated in each inset are in units of 1000 km s^{-1} relative to the core. The velocity of the core is indicated by the vertical line in each inset and is based on the line centroid of the $[\text{OIII}]\lambda 5007$ emission line within the core. North is at the top, and east is to the left in this image.

km s^{-1} . The latter value might be somewhat influenced by a night sky line residual.³ We will therefore use the average of $\Delta v_{\text{knot}2}$ and $\Delta v_{\text{knot}3}$ to estimate the rotation velocity in the peripheral regions of the arc+core galaxy, $v_{\text{rot}} \sim 190 \text{ km s}^{-1}$.

³We only state observed velocities, and do not correct for inclination with the line of sight (i_{los}), because of the large uncertainties related to geometrical distortions of the $\mathcal{M} = 20$ gravitational lens. Moreover, the lensing implies another correction factor $\sin(i_{\text{lens}})$, to account for the inclination between the kinematic major axis of the arc+core galaxy and the magnification axis. All relative velocities in this paper are therefore projected velocities, $v_{\text{obs}} = \sin(i_{\text{los}}) \sin(i_{\text{lens}}) v_{\text{intrinsic}}$.

4.1. Evidence for Disk Rotation at $z = 3.2$

We show the velocity curve of the arc+core in Fig. 3. Unfortunately, both the cluster potential and influence of nearby galaxies are not known accurately enough to allow for a robust magnification estimate. Thus in Fig. 3 we show the velocity curve for a range of assumed magnifications to illustrate this relative uncertainty. Velocities in the arc+core decrease monotonically from South to North in the core (i.e., within the central ~ 1 kpc) and arc (over a distance of $\sim 6''$ or 2.5 kpc). Thanks to the large magnification and bright line emission in the core, we can trace the velocity gradient even within the core over $2.3''$, or ~ 6 seeing disks, so correlations due to overlapping seeing disks within the data are negligible. Moreover, this causes the ratio of velocity gradient $v_{rot} \sim 190$ km s $^{-1}$ and central velocity dispersion, $\sigma_{core} \sim 70$ km s $^{-1}$, $v/\sigma \lesssim 3$, to not depend on seeing. We overlay the rotation curve for the local galaxy, NGC4419 (Fig. 3). This shows indeed that the velocity curve of the arc+ core is very similar to that of local nearby galaxies like NGC4419. NGC4419 was chosen for this purpose because its asymptotic velocity matches that measured for the arc+core particularly well.

4.2. Alternative Models: The AGN, Wind, and Merger Hypothesis

Due to the anisotropic lensing, we cannot use the full two-dimensional velocity field of the arc+core galaxy to distinguish rotation from alternative models of the origin of the line emission such as an AGN or starburst driven wind, or a merger of two galaxies. We therefore base our arguments on the whole of the rest-frame UV (Mehlert et al. 2001) and optical (this paper) spectral properties.

For a luminous AGN we would expect several characteristic bright emission lines in the rest-frame UV spectrum, such as NV λ 1240, SiIV+O IV] λ 1400, CIV λ 1549, C III]+SiIII] λ 1900, etc. Instead Mehlert et al. (2001) observe an absorption line spectrum which is typical of an actively star-forming high-redshift galaxy. The optical emission lines are narrow, FWHM $\sim 150 - 160$ km s $^{-1}$ (see Table 2), with constant (within the uncertainties) line profiles, line ratios ([OIII]/H β), and equivalent widths across both the arc and core. None of these properties provides an indication of the arc+core galaxy hosting a UV/optically bright AGN

If the kinematics of the emission line gas were dominated by superwinds (e.g., Lehnert & Heckman 1996a), one would not expect the line emission to have the same morphology as the bright continuum emission. Line emission in the arc+core galaxy generally follows the continuum morphology, arguing against the superwind hypothesis. To quantify this,

we have compared the equivalent widths in the arc+core with a sample of 12 low redshift, low metallicity galaxies with active star-formation taken from Storchi-Bergmann et al. (1995). Rest-frame $H\beta$ and $[\text{OIII}]\lambda 5007$ equivalent widths in the arc and core are for $H\beta$ and $[\text{OIII}]\lambda 5007$, respectively, $W(H\beta)_{arc} = 22 \text{ \AA}$, $W(H\beta)_{core} = 46 \text{ \AA}$, $W([\text{OIII}]\lambda 5007)_{arc} = 89 \text{ \AA}$, $W([\text{OIII}]\lambda 5007)_{core} = 171 \text{ \AA}$. These values are within the broad range of equivalent widths measured in the integrated spectra of the low redshift sample of Storchi-Bergmann et al. where the line emission is not dominated by superwinds.

$[\text{OIII}]\lambda 5007/H\beta$ line ratios increase by up to 1 dex with increasing distance from the galactic disk in galaxies exhibiting superwinds due to the (relative) dominance of shock ionization at large distances from the disk (e.g. Dahlem et al. 1997; Moran et al. 1999), even when a strong wind is projected onto the galaxy continuum (Devost et al. 1997, measure a variation of 0.3 dex in in the low metallicity dwarf galaxy, NGC1569). The arc and core span a few kpc in the source plane, so that we would expect a change in line ratios if the emission was arising from the wind. We find however insignificant differences in $[\text{OIII}]/H\beta$ line ratios, $([\text{OIII}]/H\beta)_{arc} = 2.53$ and $([\text{OIII}]/H\beta)_{core} = 2.48$ in the arc and core, respectively. This of course does not imply the general absence of a superwind in this galaxy, it only indicates that the cores of the optical emission lines are not dominated by an outflow. We find a similar situation in the $z=2.57$ strongly star-forming submillimeter galaxy SMMJ14011+0252 (Nesvadba et al. 2006, in preparation).

To investigate whether the kinematics of the arc+core could be due to a merger, we have constructed a Monte Carlo simulation, evaluating the likelihood that two unrelated LBGs have similar R-G colors as that observed by Mehlert et al. (2001) for the arc and core. To make this comparison, we used the R-G color distribution of Shapley et al. (2001) as reference distribution for the colors of LBGs. In 95% of all cases, color differences between two random pairs of LBGs are larger than $\Delta(R-G)=0.39$ – the 1σ uncertainty of the R-G color difference between the arc and the core. Moreover, the light distribution appears very smooth and contiguous in the ACS image with $\lesssim 0.1''$ resolution. This means that either the light profiles of two merging galaxies would have to overall be very similar, or that their physical separation would have to be less than ~ 40 pc. Given the regularity of the surface brightness distribution in the ACS image (Fig. 1), this seems highly unlikely. The uniform line widths and $[\text{OIII}]/H\beta$ ratios in the arc and core indicate similar gravitational potentials and overall gas ionization (excitation and metallicity). In addition, if this were a merger, then the absence of obvious irregularities in the velocities and line widths as a function of projected position would be puzzling given the high physical resolution due to the strong lensing and the reasonable number of independent resolution elements across the arc+core. Moreover, the good agreement of the position velocity diagram with the rotation curve of NGC4419 requires that the velocity difference, rotation speeds, positions and relative orientation of

two merging galaxies are very well matched. This fine tuning of several degrees of freedom makes the merger scenario highly unlikely.

5. Dynamics and evolutionary stage

5.1. Dynamical Mass Estimates and Mass Surface Density

Sofue et al. (2003) studied the properties of rotation curves of nearby disk galaxies and found that low-mass spiral galaxies tend to rotation speeds that increase out to larger radii (up to several kpc) than do the more massive disk galaxies. However, the rotation curves of most galaxies, regardless of mass, appear to rise out to a few hundred parsecs and this rise corresponds roughly to the region consisting of the bulge of the galaxy. In Fig. 3, we show the high-resolution CO rotation curve of the nearly edge on ($i \sim 80^\circ$) NGC4419, a dwarf SBa galaxy in the Sofue et al. (2003) sample with a very similar position-velocity diagram as the arc+core. If the magnification in the arc does not strongly exceed the $\mathcal{M} = 20$, then the two curves agree remarkably well.

Although this excellent agreement is coincidental, it is illustrative to compare the properties of the arc+core galaxy and NGC4419. The mass of NGC4419 within $r = 0.5$ kpc is $M_{dyn} \sim 1.7 \times 10^9 M_\odot$, whereas at $r = 2$ kpc, the enclosed mass is $M_{dyn} \sim 5 \times 10^9 M_\odot$ (Sofue et al. 2003). As noted earlier, this does emphasize that interpreting the velocity curve of the arc+core as a rotation curve is justifiable. More specifically, the ACS morphology and velocity gradient of the arc+core galaxy are at least consistent with the assumption that this is a disk galaxy seen nearly edge-on.

We fit the velocity curve of the core with a simple exponential disk model, accounting for the seeing, magnification by the gravitational lens ($\mathcal{M} = 20$), and coarse sampling of our data. The simulated data were extracted in the same way as our observational data. We obtain a robust fit for a mass of $M_{dyn,0.5kpc} = 1.3 \times 10^9 M_\odot$ within a radius $R = 0.5$ kpc, assuming an edge-on thin disk parallel to the lensing axis with no bulge, and similar disk scale-length as the typical LBG at $z \approx 3$. Extrapolating this fit out to $R = 2.3$ kpc (the typical half-light radius of $z \sim 3$ LBGs, Giavalisco, Steidel, & Macchetto 1996), we find $M_{dyn,2.3kpc} \sim 5 \times 10^9 M_\odot$. Since it is difficult to place firm constraints on the inclination, we leave it unconstrained, and only note that, statistically, the mass will be a factor of 2 higher. We also measure a relatively large velocity dispersion in the core. If the dispersion is indeed due to the gravitational potential, then a significant part of the total kinetic energy might be in random motions, adding another factor $\lesssim 2$ to the true dynamical mass (or $\lesssim 10^{10} h_{70}^{-1} M_\odot$). Our mass estimate suggests a somewhat lower mass than the $M_{dyn,CO} \sim 10^{10} h_{70}^{-1} M_\odot$.

mass of the lensed $z = 2.7$ LBG MS1512-cB58 that Baker et al. (2004) estimate from CO line width, but agrees within factors of a few. It is also consistent with estimates of LBG masses based on emission line velocity dispersions (such as, e.g., the $\langle M_{dyn} \rangle \sim 1.3 \times 10^{10} h_{70}^{-1}$ estimate of Pettini et al. 2001, assuming a pressure-supported spheroidal mass distribution). The agreement becomes better if we apply the method of Pettini et al. (2001) and measured velocity dispersions in the arc+core. Using the $\sigma \sim 70 \text{ km s}^{-1}$ of the high surface-brightness core (which would dominate the spectrum if the source was not gravitationally lensed), we estimate a dynamical mass $M_{dyn,P01}^{core} \approx 3 \times 10^{10} M_{\odot}$ ($M_{dyn,P01}^{arc+core} \approx 7 \times 10^{10} h_{70}^{-1} M_{\odot}$, if we use the integrated line emission from the arc and the core.) Given that we are estimating the dynamical mass within roughly a half-light radius for the typical LBG at $z \sim 3$, it also agrees well with the mass estimates based on SED fitting (Shapley et al. 2001). Since $z \sim 3$

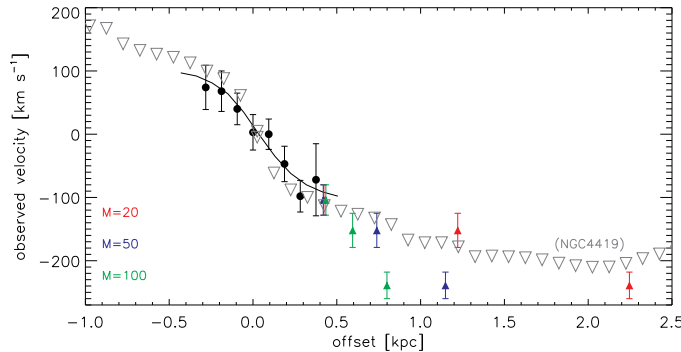


Fig. 3.— [OIII] $\lambda 5007$ Position-peak velocity curve of the core and arc. Data in the core are shown as black dots, triangles indicate the velocities in the arc for different magnifications (red – $\mathcal{M} = 20$, blue – $\mathcal{M} = 50$, green – $\mathcal{M} = 100$). Gray upside-down triangles indicate the digitized rotation curve of NGC4419 taken from Sofue et al. (2003), the black line shows our best-fit elliptical disk model (for the core only).

LBGs have co-moving densities similar to local luminous ($\mathcal{L} \gtrsim \mathcal{L}^*$) galaxies, high star-formation rates, and complex morphologies, Steidel et al. (1996) argued that they represent the formation of the spheroidal component of massive galaxies. Our results have some bearing on this issue. The similarity with the rotation curves of local spiral galaxies, e.g., NGC4419, comprises the rise and overall shape within $\sim 1 \text{ kpc}$ radius, where we have a robust lensing model, and out to $\lesssim 2.5 \text{ kpc}$ with somewhat larger uncertainties related to the higher magnification. The low-redshift, $\sim \mathcal{L}^*$ galaxies in Sofue et al. (2003) have an average (and rms) mass within 0.5 kpc of $2.9 \pm 2.0 \times 10^9 M_{\odot}$ (which range from $\approx 10^8$ to $7 \times 10^9 M_{\odot}$), similar to our $M_{dyn,0.5kpc} \sim 2 \times 10^9 M_{\odot}$, including the statistical inclination correction. Obviously, due to the similar rotation velocities and sizes, the mass surface densities of the core and local comparison sample are also very similar: $3 \times 10^3 M_{\odot} \text{ pc}^{-2}$ for the core and $3.7 \pm 2.6 \times 10^3$

$M_{\odot}\text{pc}^{-2}$ for the average and rms in the Sofue et al. sample.

These similarities lend support to the conclusion of Steidel et al. (1996) that in fact LBGs could be the inner spheroid component during a period of rapid growth. More subtly, this implies that perhaps the full mass of the central few kpcs (bulges?) of present-day $\sim \mathcal{L}^*$ galaxies was already in place by $z \gtrsim 3$. Given the results of Baker et al., the central few kpc are probably mostly in a gaseous phase and not a complete stellar bulge. We discuss these hypotheses in more detail below.

5.2. Stellar population, star-formation rates and chemical enrichment

We constrain the stellar population from the rest-frame UV spectrum of Mehlert et al. (2001). A detailed assessment of the UV absorption line spectrum is difficult because of inadequate signal-to-noise ratio and strong night sky lines at the wavelengths of some of the important diagnostic absorption lines. However, we obtain a good fit to the overall spectral energy distribution for rest-frame UV wavelengths between $\sim 1000 - 2000 \text{ \AA}$ using STARBURST99 (Leitherer et al. 1999) for a model with a 60-110 Myr old stellar population and low extinction. Our data are not sufficient to explicitly measure the extinction. In the following, we therefore use the average $E(B-V)=0.17$ found by Shapley et al. (2001) for a sample of $z \sim 3$ LBGs with similar $\text{Ly}\alpha$ emission line equivalent width, although our SED fitting formally suggests no extinction.

Such a model correctly predicts the K-band continuum magnitude we observe with SPIFFI ($K=20.5\pm 0.3$), and implies a stellar mass $M_{\text{stellar}} \sim 2-7 \times 10^9 \mathcal{M}^{-1} M_{\odot}$. Convolution of the Mehlert et al. (2001) spectrum with the filter transmission curves of Steidel et al. (2003) to select Lyman break galaxies verifies that the arc+core formally fulfills the color criterion for $z \sim 3$ LBGs (including the fact that the lensing-corrected magnitude fulfill the spectroscopic $R = 25.5$ magnitude limit used in selecting LBGs by Steidel and collaborators; Steidel et al. 2003). In Table 1 we compare the measured properties of the arc+core galaxy with averages of the general LBG population, which indicates the arc+core is in fact a LBG.

The mass-to-light ratio $M_{\text{dyn}}/\mathcal{L}_B$ sets powerful constraints on the nature of a stellar system. Assuming a typical $E(B-V)=0.17$ mag (Shapley et al. 2001) for the arc+core galaxy, we find $M_{\text{dyn}}/\mathcal{L}_B \sim 0.4M_{\odot}/\mathcal{L}_{\odot}$, correcting for a magnification $\mathcal{M} = 20$. This $M_{\text{dyn}}/\mathcal{L}_B$ is consistent with a ~ 200 Myr old stellar population. The gross agreement between $M_{\text{dyn}}/\mathcal{L}_B$ and the age derived from fitting the UV continuum indicates that the total uncertainties in our dynamical mass estimates and the gravitational magnification cannot be off by more than factors of a few.

Since our rest-frame optical data and the rest-frame UV spectroscopy of Mehlert et al. (2001) do not indicate the presence of an AGN, we can use the measured integrated $H\beta$ flux of the arc+core galaxy, $F(H\beta) = 6.7 \times 10^{-17}$ ergs s^{-1} cm^{-2} (see Table 2) to estimate the star-formation rate. Assuming a magnification factor $\mathcal{M} = 20$ and an intrinsic ratio of $H\alpha/H\beta = 2.75$, we estimate a star-formation rate $SFR \sim 11 M_{\odot} \text{ yr}^{-1}$ for the arc+core, but with considerable uncertainty. If using a more realistic IMF (e.g., a Kroupa IMF) instead of the calibration of Kennicutt (1998) with mass limits of $0.1 M_{\odot}$ to $100 M_{\odot}$ for a Salpeter IMF, the star-formation rate would be about a factor of 1.6 to 2.5 lower. However, the intrinsic $H\beta$ flux might be somewhat higher, because parts of the galaxy might not be lensed (especially in the periphery) or we have not observed every lensed component. Moreover, $H\beta$ might suffer strong underlying absorption from the stellar population with an age of ~ 100 Myr.

We also constrain the gas-phase oxygen abundance, based on the classical R_{23} estimator ($R_{23} \equiv (I([OII]\lambda 3727) + I([OIII]\lambda\lambda 4959, 5007))/H\beta$; Pagel et al. 1979). Since we have not measured $[OII]\lambda 3727$, we use the correlation of $[OII]\lambda 3727/[OIII]\lambda 5007$ with $[OIII]\lambda 5007/H\beta$ given by Kobulnicky et al. (1998) for low-metallicity galaxies to estimate the most likely $[OII]\lambda 3727$ flux. We measure $[OIII]/H\beta = 3.9$, corresponding to an upper limit of $\log [OIII]\lambda 5007/H\beta = 0.59 \pm 0.14$, and $\log R_{23}^{\text{est}} = 0.99 \pm 0.2$, if we include the average $\log [OII]\lambda 3727/H\beta = 0.4 \pm 0.15$ of Kobulnicky et al. (1998). This corresponds to an oxygen abundance of $12 + \log [O/H] = 8.34_{-0.34}^{+0.26}$, including all uncertainties and the double valued nature of R_{23} . Relative to the solar oxygen abundance of Allende Prieto, Lambert, & Asplund (2001), the best-fit value corresponds $[\frac{O}{H}] \equiv \log [\frac{O}{H}] - \log [\frac{O}{H}]_{\odot} = -0.4 \pm 0.3$. Mehlert et al. (2002) estimated the metallicity of the core from the CIV $\lambda 1550$ rest-frame equivalent width, $W_{CIV}^0 = 2.01 \pm 0.63 \text{ \AA}$. Accounting for uncertainty in their measurement, ~ 0.3 dex scatter in their abundance calibration, and a different solar oxygen abundance, their CIV equivalent width implies an oxygen abundance of $[\frac{O}{H}] = -1.0 \pm 0.4$. Both abundance estimates agree within 1σ .

6. Dynamical Time, Evolutionary State, and Angular Momentum

By combining the star-formation rate and kinematic measurements, we can constrain the evolutionary state of the inner region of the 1E0657-56 core. The observed relative velocities imply an orbital timescale of:

$$t_{orb} = 2\pi R/V_{circ} = 30 \left(\frac{v_{circ}}{100 \text{ km s}^{-1}} \right)^{-1} \left(\frac{R}{500 \text{ pc}} \right) h_{70} \text{ Myrs} \quad (1)$$

Starbursts in local galaxies typically last for several orbital timescales (e.g., Lehnert & Heckman 1996b; Kennicutt 1998; Förster Schreiber, Genzel, & Lutz 2003), about 10 to a few 100 Myrs. Generally speaking, LBGs have properties similar to low redshift starburst galaxies (e.g., Meurer et al. 1997), and given that the core has a similar orbital time, by analogy, we assume that the LBG phase will have a similar length. This limits the total length of the starburst in the 1E0657-56 “core” to a few 100 Myrs. Of course, it may already be at the end of its burst – the dynamical estimate only sets a likely upper limit.

Our result agrees with what little is known about the molecular gas content of LBGs. Baker et al. (2004) found a large reservoir of molecular gas in the lensed $z = 2.7$ LBG MS1512-cB58, sufficient to sustain intense star-formation over several orbital time scales. E.g., assuming a gas fraction of $f_{gas} = 0.5M_{dyn}$, star-formation at a rate of $11 M_{\odot} \text{ yr}^{-1}$ could be sustained for ~ 250 Myr. From spectral energy distribution (SED) fitting of a sample of LBGs, Shapley et al. (2001) found a median star-formation time scale of ~ 300 Myrs. This is in rough agreement with our dynamical time estimate, and a few times larger than the ~ 80 Myrs we find for the age of stellar population in the arc+core. Of course this can only provide only limited support for this general argument given the degeneracies between age and extinction and the lack of a unique fit to any SED given the wide range of possible and plausible star-formation histories.

Within the context of models where galaxies grow hierarchically, angular momentum in galaxies is a result of tidal torques from neighboring mass concentrations (Peebles 1969). In (Λ) CDM, these torques are generated by merging dark matter halos (White 1984). If this hypothesis for the generation of angular momentum is correct, then our observed rotation curve in the arc+core is a direct link to the spin and specific angular momentum of the dark matter halo. We observe a significant amount of specific angular momentum in the arc+core, namely,

$$j_{arc+core} \approx 2R_d V_{circ} = 10^{2.9 \pm 0.3} \left(\frac{R}{2\text{kpc}} \right) \left(\frac{v_{circ}}{190 \text{ km s}^{-1}} \right) h_{70}^{-1} \text{ km s}^{-1} \text{ kpc} \quad (2)$$

where R_d is the e-folding radius of the light profile, and V_{circ} is the circular velocity of the disk. The light profile of the arc+core is not consistent with an exponential disk, which is perhaps not surprising given the complex lensing configuration. Ravindranath et al. (2004) find that exponential light profiles dominate their sample of $z \sim 3$ actively star-forming galaxies in the HST *Ultra Deep Field*. If the arc+core is a typical LBG, then the

magnification is likely not a simple cut along the radius of the galaxy. Therefore, we simply estimate the specific angular momentum at the approximate radius for which we have direct measurements (i.e., ~ 2 kpc, similar to the typical half-light radius of an LBG; Giavalisco, Steidel, & Macchetto 1996). The specific angular momentum is within the lower tail of the specific angular momentum distribution of local spiral galaxies ($\sim 10^{2.8-3.6} h_{70}^{-1} \text{ km s}^{-1} \text{ kpc}$ at $v_c \sim 200 \text{ km s}^{-1}$, see e.g. Abadi et al. 2003, and references therein). Although the arc+core is at the low end of the distribution, formally it is consistent, and most of the difference can be attributed to the generally larger radii over which the specific angular momenta of local disks are estimated (which for the flat part of the rotation curve increases linearly with radius). Moreover, simple models of the evolution of the angular momentum of dark matter halos predicted a decrease in angular momentum with increasing redshift ($j_{halo}(z) \propto (1+z)^{-1.5}$ for an isothermal halo with a binding energy consistent with simple kinetic theory, i.e., $E_{binding} \approx M_{halo} V_{circ}^2(r = r_{virial})$, where $V_{circ}(r = r_{virial})$ is the circular velocity of the halo at the virial radius; see Mo, Mao, & White 1998; Förster Schreiber et al. 2006).

7. Halo Mass and Baryonic “Collapse Fraction”

The large specific angular momentum observed in local disk galaxies is difficult to explain, unless by postulating that the specific angular momentum of the gas is roughly conserved during collapse and similar to the specific angular momentum of the dark matter halo. This is closely related to the well-known “angular momentum problem” and it is not a trivial issue. Given the specific angular momentum of the arc+core is similar to local spirals, we are tempted to estimate the dark matter halo mass of the arc+core galaxy from the kinematics of the emission line gas within the formalism of the hierarchical model (Förster Schreiber et al. 2006). Hypothesizing that the specific angular momentum of the arc+core approximately reflects that of the halo, would imply that we can estimate the dark matter halo mass using the observed kinematics of the arc+core. With the virial formula of, e.g., Mo, Mao, & White (1998), and the measured circular velocity over a radius of a few kpc (about 190 km s^{-1}), we find,

$$M_{halo}^{\text{arc+core}} = 10^{11.7 \pm 0.3} \left(\frac{v_c}{190 \text{ km s}^{-1}} \right)^3 h_{0.7}^{-1} \left(\frac{1+z}{4.2} \right)^{-1.5} M_{\odot} \quad (3)$$

Based on correlation amplitudes and number densities of LBGs at $\langle z \rangle = 2.9$, Adelberger et al. (2005) estimate dark matter halo masses of $\log M_{halo}/M_{\odot} \sim 11.5 \pm 0.3 M_{\odot}$,

similar, within $\sim 1\sigma$, to our estimate using the kinematics of the arc+core. This suggests that the measured circular velocity roughly approximates the virial velocity of the dark matter halo. Förster Schreiber et al. (2006) found a similar result in a study of UV-selected galaxies at $z\sim 2$.

We find a low dynamical mass for the arc+core compared to the large dark matter halo mass, but within the range of dynamical masses that Pettini et al. (2001) found for a larger sample of LBGs with measured velocity dispersions. This indicates that in the general LBG population, only a small fraction of the total available baryons have likely collapsed to the center of the halo. Our best-fit mass estimate for the arc+core is $\log M_{dyn,2kpc}/M_\odot = 9.5\pm 0.3$ M_\odot within $R \sim 2$ kpc (i.e., within a typical half-light radius of an LBG at $z\sim 3.2$, see Bouwens et al. 2004; Giavalisco, Steidel, & Macchetto 1996), which implies a log ratio of baryonic to dark mass of -2.2 ± 0.4 dex or ~ 0.3 to 2%. This is actually a lower limit since we have not accounted for a contribution of dark matter within 2 kpc of the dynamical center.

We can use results from the literature to repeat this comparison with a complementary approach, in analogy to the analysis of Adelberger et al. (2005) for $z \sim 2$ UV-selected star-forming galaxies (“BM/BX”). Using the $\log M_{halo}/M_\odot \sim 11.5 \pm 0.3$ halo mass deduced from the measured large-scale distribution and the typical stellar mass of $z \sim 3$ LBGs derived from multi-color photometry, $\log M_\star/M_\odot = 9.9 \pm 0.3$ (Shapley et al. 2001), we find a ratio of baryonic to dark matter masses of $\log M_\star/M_{halo} = -1.6 \pm 0.4$ or 1-6%. Given the large uncertainties in any such estimate, this is in good agreement with the proceeding results based on dynamical mass estimates.

The best-fitting cosmological parameters imply that the fraction of baryonic to total mass is about $\Omega_b/\Omega_m \approx 0.17$ (e.g., Spergel et al. 2003). If we take our estimates literally, then this will imply that only $\sim 2 - 10\%$ of the baryons in a typical $z\sim 3$ LBG have already collapsed to $\sim r_e$. For the Milky Way, the ratio of total baryonic to dark mass is 0.08 ± 0.01 (e.g., Cardone & Sereno 2005). Adelberger et al. (2005) and Förster Schreiber et al. (2006) find a value similar to the Milky Way in the $z \sim 2$ “BM/BX” galaxies. The halos of the Milky Way and the BM/BX galaxies have very similar mass and exceed the typical mass of a $z \sim 3$ LBG halo by only about a factor 3 (Adelberger et al. 2005).

Finding such a low value in comparison with other galaxy populations at low and high redshift implies that the “baryonic collapse fraction” of $z \sim 3$ LBGs is generally lower. This suggests that LBGs perhaps formed relatively inefficiently or have particularly strong feedback making the collapse appear relatively inefficient. Direct evidence for LBGs having significant outflows is substantial (Adelberger et al. 2003; Shapley et al. 2003), supporting the later hypothesis. The rather small differences in the halo masses and large differences in the collapse fraction might be evidence that the collapse of baryons or feedback have a

strong impact on galaxy evolution in general, and that merging of dark matter halos is not the only significant parameter in determining the characteristics of galaxies.

8. Summary and A Plausible Evolutionary Scenario for LBGs

We presented an analysis of the strongly lensed ($\mathcal{M} = 20$) Lyman break galaxy 1E0657-56 arc+core galaxy at redshift $z = 3.24$, based on SPIFFI integral-field rest-frame optical spectroscopy, complemented with rest-frame UV imaging and spectroscopy. This galaxy is an excellent target for studying the fine spatial details of a $z \sim 3$ Lyman break galaxy. We extracted the rest-frame UV colors of the arc+core from the deep FORS spectroscopy of Mehlert et al. (2001), and measured directly that the galaxy fulfills the Lyman break criterion, including the $R = 25.5$ mag limit, imposed on spectroscopically identified sources, for an unlensed source. The arc+core is near the peak of the LBG redshift distribution, and its unmagnified size, optical emission line properties, mass-to-light ratio, and stellar age are within the range estimated for the overall population. Therefore, it is particularly well suited for a detailed analysis of its small-scale properties. We find a slightly lower star-formation rate than average, most likely due to our uncertain extinction estimate, likely underlying $H\beta$ absorption, or missing flux by not accounting for unlensed or multiply lensed regions of the galaxy.

Through studying magnified high surface brightness regions of an LBG at $z \sim 3$, we can investigate the structure and nature of LBGs at high physical resolution. The dynamical mass within 500 pc is about $2 \times 10^9 M_{\odot}$, while at about 2 kpc radius (approximately the half-light radius of a typical $z \sim 3$ LBG, e.g., Giavalisco, Steidel, & Macchetto 1996), the mass is similar to the average stellar mass $\sim 10^{10} M_{\odot}$ of LBGs. Stellar masses derived from SED modelling include light at larger radii and make assumptions about the initial mass function that may be unwarranted and generally lead to higher masses (Förster Schreiber et al. 2006), so any discrepancy is not totally unexpected. However, our estimated mass of the core is also typical for the bulges of local $\sim \mathcal{L}^*$ spiral galaxies. In addition, the arc+core has a specific angular momentum similar to that of local spiral galaxies.

The combination of mass surface density, metallicity and the dynamical time perhaps suggests an interesting evolutionary picture for the 1E0657-56 arc+core. Since the properties of the 1E0657-56 arc+core are well within the typical range of LBGs, this outline of the evolution of the 1E0657-56 arc+core might, with some caution, be applicable to $z \sim 3$ LBGs generally.

Compared to local spirals, most of the mass within 500 pc for the 1E0657-56 core

appears to be already in place. However, the metallicity in the nuclei of low-redshift spirals is approximately solar, while we have found that the 1E0657-56 arc+core has at most about half solar gas-phase abundances, and this estimate is clearly dominated by the emission from the core. We do not know the gas fraction of the 1E0657-56 arc+core, however, CO observations of the lensed $z=2.7$ LBG MS1512-cB58 by Baker et al. (2004) suggest that LBGs might be gas rich, with gas fractions of possibly up to 50%. For a simple closed box model with such high gas fractions, the metallicity will double within several 10 to 100 Myrs. This time estimate likely increases by factors of a few if including outflows or inflows with the metallicity of the intergalactic medium at $z \sim 3$. Our orbital time estimate suggests that the intense star-formation is likely to last long enough to increase the metallicity to about solar.

Because $z \sim 3$ LBGs have similar co-moving densities as local luminous ($\mathcal{L} \gtrsim \mathcal{L}^*$) galaxies, Steidel et al. (1996) suggested that they represent the formation of the spheroidal component of massive galaxies. Our analysis suggests that this hypothesis is plausible since we measure a mass and mass surface density similar to local $\sim \mathcal{L}^*$ spiral galaxies, and also fulfill the metallicity constraint, after allowing for further evolution in the on-going episode of intense star-formation. Moreover, the low baryon collapse fraction within $\sim r_e$ might hint that a substantial amount of gas resides on larger scales within the halo (maybe gas blown out during intense star-formation or pre-enriched material from the IGM). However, we also find $v_c/\sigma \lesssim 3$, significantly larger than the $v_c/\sigma \sim 0 - 1.2$ of bulges (Kormendy & Kennicutt 2004, and references therein). Thus, if the arc+core is representative of the overall population, LBGs will have to lose factors of a few in their circular velocities to have v_c/σ ratios consistent with local bulges, and certainly substantially more angular momentum to evolve into massive ellipticals.

Currently, very few models address the evolution of individual disk galaxies within the context of the hierarchical model in detail, which makes a quantitative comparison rather difficult. Overall, models of the formation of large scale structure and the evolution of galaxies within a Λ CDM cosmology favour “inside-out” galaxy evolution, where the inner regions of galaxies form earlier than the peripheries (e.g., Samland & Gerhard 2003; Abadi et al. 2003). Such a scenario quite naturally explains observations at low redshift, such as metallicity and stellar population (age) gradients observed in local galaxies.

Although these models produce inner regions of galaxies that collapse relatively early, unfortunately they also predict that only a relatively small amount of mass will be in place by $z \sim 3$ compared to the final mass of the galaxy. Most of the mass at small radii is acquired rather late, more likely around redshifts of-order $z = 1$ (Samland & Gerhard 2003). However, as emphasized by Immeli et al. (2004), the timing and spatial distribution of the

star-formation “history” depends crucially on the infall history and on how efficiently the kinetic energy gained from dynamical and mechanical heating during collapse is dissipated. They show that the gas in galaxies with large dissipation efficiency will strongly fragment, and interactions between individual subclumps and dynamical friction will make the fragments coalesce to the central regions more rapidly. In other words, the efficiency of dissipation and fragmentation may essentially be a free parameter which could be constrained observationally.

In comparison to local \mathcal{L}^* spiral galaxies, we find in the arc+core at $z = 3.2$ a significant and comparable mass surface density, while the overall relative mass is rather low. In light of the models already discussed, this might indicate highly dissipative gas collapse during the earliest phases of galaxy evolution. The later evolution and perhaps the formation of the disk might either be driven by infall of material (e.g., Samland & Gerhard 2003) or by the merger of gas rich galaxies supported by strong feedback to prevent the baryons from collapsing into the central regions (e.g., Robertson et al. 2005). The latter of these hypotheses might explain the apparent inefficiency of the baryon collapse of the $z \sim 3$ LBGs compared to galaxies at lower redshift.

We would like to thank the SPIFFI team for carrying out the observations and C. Forman-Jones for responding to our request for data so promptly and to her and her collaborators for sharing their reduced ACS data with us before publication.

REFERENCES

- Abadi, M. G., Navarro, J. F., Steinmetz, M., & Eke, V. R. 2003, *ApJ*, 591, 499
- Allende Prieto, C., Lambert, D. L., & Asplund, M. 2001, *ApJ*, 556, L63
- Adelberger, K. L., Steidel, C. C., Giavalisco, M., Dickinson, M., Pettini, M., & Kellogg, M. 1998, *ApJ*, 505, 18
- Adelberger, K. L., Steidel, C. C., Shapley, A. E., & Pettini, M. 2003, *ApJ*, 584, 45
- Adelberger, K. L., Steidel, C. C., Pettini, M., Shapley, A. E., Reddy, N. A., & Erb, D. K. 2005, *ApJ*, 619, 697
- Appenzeller, I., et al. 1998, *The Messenger*, 94, 1
- Baker, A. J., Tacconi, L. J., Genzel, R., Lehnert, M. D., & Lutz, D. 2004, *ApJ*, 604, 125

- Bender, R., Burstein, D., & Faber, S. M. 1993, *ApJ*, 411, 153
- Borys, C., et al. 2004, *MNRAS*, 352, 759
- Bouwens, R. J., Illingworth, G. D., Blakeslee, J. P., Broadhurst, T. J., & Franx, M. 2004, *ApJ*, 611, L1
- Cardone, V. F., & Sereno, M. 2005, *A&A*, 438, 545
- Dahlem, M., Petr, M. G., Lehnert, M. D., Heckman, T. M., & Ehle, M. 1997, *A&A*, 320, 731
- Devost, D., Roy, J.-R., & Drissen, L. 1997, *ApJ*, 482, 765
- Eisenhauer, F., Tecza, M., Mengel, S., Thatte, N. A., Roehrle, C., Bickert, K., & Schreiber, J. 2000, *Proc. SPIE*, 4008, 289
- Elmegreen, B. G. 2005, Elmegreen, D. M., Vollbach, D. R., Foster, E. R., Ferguso, T. E., *ApJ*, in press, astro-ph/0510245
- Förster Schreiber, N. M., Genzel, R., & Lutz, D. 2003, *ApJ*, 599, 193
- Förster Schreiber et al. 2006, submitted to *ApJ*
- Fosbury, R. A. E., et al. 2003, *ApJ*, 596, 797
- Franx, M., Illingworth, G. D., Kelson, D. D., van Dokkum, P. G., & Tran, K. 1997, *ApJ*, 486, L75
- Gialalisco, M., Steidel, C. C., & Macchetto, F. D. 1996, *ApJ*, 470, 189
- Heckman, T. M., Robert, C., Leitherer, C., Garnett, D. R., & van der Rydt, F. 1998, *ApJ*, 503, 646
- Immeli, A., Samland, M., Gerhard, O., & Westera, P. 2004, *A&A*, 413, 547
- Kennicutt, R. C. 1998, *ARA&A*, 36, 189
- Kobulnicky, H. A., Kennicutt, R. C., Jr., & Pizagno, J. 1998, *ApJ*, 514, 544
- Kormendy, J. & Kennicutt, R. 2004, *ARA&A*, 42, 603
- Krist, J. E., & Hook, R. N. 1997, *The 1997 HST Calibration Workshop with a New Generation of Instruments*, p. 192, 192

- Lehnert, M. D. & Heckman, T. M. 1996a, *ApJ*, 462, 651
- Lehnert, M. D. & Heckman, T. M. 1996b, *ApJ*, 472, 546
- Leitherer, C., et al. 1999, *ApJS*, 123, 3
- Lemoine-Busserolle, M., Contini, T., Pelló, R., Le Borgne, J.-F., Kneib, J.-P., & Lidman, C. 2003, *A&A*, 397, 839
- Mehlert, D., et al. 2001, *A&A*, 379, 96
- Mehlert, D., et al. 2002, *A&A*, 393, 809
- Meurer, G. R., Heckman, T. M., Lehnert, M. D., Leitherer, C., & Lowenthal, J. 1997, *AJ*, 114, 54
- Mo, H. J., Mao, S., & White, S. D. M. 1998, *MNRAS*, 295, 319
- Moran, E. C., Lehnert, M. D., & Helfand, D. J. 1999, *ApJ*, 526, 649
- Pagel, B. E. J., Edmunds, M. G., Blackwell, D. E., Chun, M. S., & Smith, G. 1979, *MNRAS*, 193, 219
- Papovich, C., Dickinson, M., & Ferguson, H. C. 2001, *ApJ*, 559, 620
- Peebles, P. J. E. 1969, *ApJ*, 155, 393
- Pettini, M., Shapley, A. E., Steidel, C. C., Cuby, J., Dickinson, M., Moorwood, A. F. M., Adelberger, K. L., & Giavalisco, M. 2001, *ApJ*, 554, 981
- Ravindranath, S., Ferguson, H., Giavalisco, M., Dickinson, M., Papovich, C., & GOODS 2004, American Astronomical Society Meeting Abstracts, 205,
- Pettini, M., Rix, S. A., Steidel, C. C., Adelberger, K. L., Hunt, M. P., & Shapley, A. E. 2002, *ApJ*, 569, 742
- Rix, H.-W., Guhathakurta, P., Colless, M., & Imig, K. 1997, *MNRAS*, 285, 779
- Robertson, B., Hernquist, L., Bullock, J. S., Cox, T. J., Di Matteo, T., Springel, V., & Yoshida, N. 2005, *astro-ph/0503369*
- Samland, M. & Gerhard, O. E. 2003, *A&A*, 399, 961
- Shapley, A. E., Steidel, C. C., Adelberger, K. L., Dickinson, M., Giavalisco, M., & Pettini, M. 2001, *ApJ*, 562, 95

- Shapley, A. E., Steidel, C. C., Pettini, M., & Adelberger, K. L. 2003, *ApJ*, 588, 65
- Sofue, Y., & Rubin, V. 2001, *ARA&A*, 39, 137
- Sofue, Y., Koda, J., Nakanishi, H., & Onodera, S. 2003, *PASJ*, 55, 59
- Spergel, D. N., et al. 2003, *ApJS*, 148, 175
- Steidel, C. C., Giavalisco, Pettini, M., Dickinson, M., & Adelberger, K. L. 1996, *ApJ*, 462, L17
- Steidel, C. C., Adelberger, K. L., Giavalisco, M., Dickinson, M., Pettini, M. 1999, *ApJ*, 519, 1
- Steidel, C. C., Hunt, M. P., Shapley, A. E., Adelberger, K. L., Pettini, M., Dickinson, M., & Giavalisco, M. 2002, *ApJ*, 576, 653
- Steidel, C. C., Adelberger, K. L., Shapley, A. E., Pettini, M., Dickinson, M., & Giavalisco, M. 2003, *ApJ*, 592, 728
- Storchi-Bergmann, T., Kinney, A. L., & Challis, P. 1995, *ApJS*, 98, 103
- Swinbank, A. M., Bower, R. G., Smith, G. P., Smail, I., Kneib, J.-P., Ellis, R. S., Stark, D. P., & Bunker, A. J. 2006, *MNRAS*, 368, 1631
- Teplitz, H. I., et al. 2000, *ApJ*, 542, 18
- Tody, D. 1993, *ASP Conf. Ser.* 52: *Astronomical Data Analysis Software and Systems II*, 2, 173
- Tucker, W., et al. 1998, *ApJ*, 496, L5
- White, S. D. M. 1984, *ApJ*, 286, 38
- Yee, H. K. C., Ellingson, E., Bechtold, J., Carlberg, R. G., & Cuillandre, J.-C. 1996, *AJ*, 111, 1783

Table 1. Properties of the arc core relative to the LBG population

	arc+core	<LBG>	reference
redshift	3.24	3.16 ± 0.12	P01
r_e [arcsec]	$0.1''\text{-}0.6''^a$	$0.3''$	G02
$\sigma_{[OIII]}$ [km s ⁻¹]	68 ± 4	73 ± 28	P01
R [mag]	$24.2 \pm 0.01^b, ^d$	24.7 ± 0.9	S03
age [10 ⁶ yrs]	80	50-100	S01
SFR [M _⊙ yr ⁻¹]	10^c	39 ± 23^c	P01
12+[O/H]	8.3 ± 0.3	8.24 ± 0.45	P01

^aFWHM perpendicular to the magnification axis.

^bIntrinsic magnitude assuming $\mathcal{M} = 20$.

^cFrom H β with H α /H β =2.75.

^dcore only

Note. — References: P01 Pettini et al. (2001) – G02 Giavalisco, Steidel, & Macchetto (1996) – S01 Shapley et al. (2001) – S03 Steidel et al. (2003)

Table 2. Emission lines in 1E0657 arc+core

zone	line	λ_{rest}	z	λ_{obs}	FWHM	FWHM _{intr.}	flux
(1)	(2)	(3)	(4)	(5)	(6)	(7)	(8)
total source	[OIII]	5007	3.2439±0.0002	2.1249±0.0001	26±2	229±21	20.038±0.7
total source	H β	4861	3.2453±0.0013	2.0637±0.0008	25±7	223±61	6.7±0.7
total arc	[OIII]	5007	3.2423±0.0004	2.1241±0.0003	23±6	146±37	4.3±0.4
total arc	H β	4861	3.2442±0.0020	2.0631±0.0013	35±34	423±413	1.7±0.4
total core	[OIII]	5007	3.2446±0.0001	2.1253±0.0005	24±1	160±8	11.7±0.2
total core	H β	4861	3.2451±0.0012	2.0635±0.0008	30±18	334±201	4.7±0.2
arc 1	[OIII]	5007	3.2433±0.0004	2.1246±0.0003	–	–	6.4±0.1
arc 1	H β	4861	3.2460±0.0010	2.0640±0.0006	–	–	1.75±0.6
arc 2	[OIII]	5007	3.2427±0.0004	2.1243±0.0003	–	–	2.73±0.5
arc 2	H β	4861	3.2438±0.0010	2.0629±0.0007	–	–	1.48±0.4
arc 3	[OIII]	5007	3.2419±0.0004	2.1239±0.0003	–	–	1.9±0.09

Note. — Column (1) – Regions as defined in Figure 2. Column (2) – Line identification. Column (3) – Rest-frame wavelengths in Å. Column (4) – Redshift for each line. Column (5) – Observed wavelengths in μm . Column (6) – Full-width at half-maximum measured in Å. Due to the faint lines in the arc and a night sky line residual which might affect the blue [OIII] λ 5007 wing, we do not give widths for the arc. Column (7) – Intrinsic FWHMs in km s^{-1} , deconvolved to account for both the spectral resolution and smoothing (by 3 pixels). Column (8) – Line fluxes in units of $10^{-20} \text{ W m}^{-2}$.